Bioactive Materials 21 (2023) 324–339

Contents lists available at ScienceDirect

Bioactive Materials

journal homepage: www.keaipublishing.com/en/journals/bioactive-materials

Bioinspired drug-delivery system emulating the natural bone healing cascade for diabetic periodontal bone regeneration

He Wang [a,1], Xiaowei Chang [b,1], Qian Ma [a], Boyang Sun [a], Han Li [a], Jinmin Zhou [a], Yiyao Hu [a], Xiaoyu Yang [a], Jie Li [a,*], Xin Chen [b,**], Jinlin Song [a,***]

[a] Chongqing Key Laboratory of Oral Diseases and Biomedical Sciences, Chongqing Municipal Key Laboratory of Oral Biomedical Engineering of Higher Education, College of Stomatology of Chongqing Medical University, Chongqing, 401147, China
[b] Department of Chemical Engineering, Shaanxi Key Laboratory of Energy Chemical Process Intensification, Institute of Polymer Science in Chemical Engineering, School of Chemical Engineering and Technology, Xi'an Jiaotong University, Xi'an, 710049, China

ARTICLE INFO

Keywords:
Periodontal bone regeneration
Diabetes mellitus
Bioinspired
Hydrogel
Drug delivery

ABSTRACT

Diabetes mellitus (DM) aggravates periodontitis, resulting in accelerated periodontal bone resorption. Disordered glucose metabolism in DM causes reactive oxygen species (ROS) overproduction resulting in compromised bone healing, which makes diabetic periodontal bone regeneration a major challenge. Inspired by the natural bone healing cascade, a mesoporous silica nanoparticle (MSN)-incorporated PDLLA (poly(DL-lactide))-PEG-PDLLA (PPP) thermosensitive hydrogel with stepwise cargo release is designed to emulate the mesenchymal stem cell "recruitment-osteogenesis" cascade for diabetic periodontal bone regeneration. During therapy, SDF-1 quickly escapes from the hydrogel due to diffusion for early rat bone marrow stem cell (rBMSC) recruitment. Simultaneously, slow degradation of the hydrogel starts to gradually expose the MSNs for sustained release of metformin, which can scavenge the overproduced ROS under high glucose conditions to reverse the inhibited osteogenesis of rBMSCs by reactivating the AMPK/β-catenin pathway, resulting in regulation of the diabetic microenvironment and facilitation of osteogenesis. *In vitro* experiments indicate that the hydrogel markedly restores the inhibited migration and osteogenic capacities of rBMSCs under high glucose conditions. *In vivo* results suggest that it can effectively recruit rBMSCs to the periodontal defect and significantly promote periodontal bone regeneration under type 2 DM. In conclusion, our work provides a novel therapeutic strategy of a bioinspired drug-delivery system emulating the natural bone healing cascade for diabetic periodontal bone regeneration.

1. Introduction

Periodontitis is a widespread oral disease that affects almost half of the adult population worldwide [1]. It continuously causes deteriorating inflammation of periodontal tissues, which leads to irreversible periodontal bone absorption and even tooth loss [2]. Moreover, periodontitis is the sixth major complication of diabetes mellitus (DM), and periodontal bone destruction is further accelerated once the patient suffers from DM [3]. In addition to accelerated periodontal bone destruction, periodontal bone regeneration was decreased by approximately 55% in type 2 DM (T2DM) [4]. In T2DM, disordered glucose metabolism causes reactive oxygen species (ROS) overproduction, affecting calcium and phosphorus metabolism. This impairs downstream pre-osteoblast migration and osteogenesis, leading to bone homeostasis disorder and compromised bone healing in diabetic patients [5,6]. Therefore, effective periodontal bone regeneration in T2DM requires the integration of ROS elimination and osteogenesis. Although a lot of biomaterials have been designed for periodontal tissue regeneration, few of them are able to resolve the problem of periodontal bone regeneration in DM [7,8].

Mesenchymal stem cells (MSCs) with osteogenic potential are essential for bone regeneration, and have been considered one of the

Peer review under responsibility of KeAi Communications Co., Ltd.
* Corresponding author.
** Corresponding author.
*** Corresponding author.
E-mail addresses: jieli@hospital.cqmu.edu.cn (J. Li), chenx2015@xjtu.edu.cn (X. Chen), songjinlin@hospital.cqmu.edu.cn (J. Song).
[1] He Wang and Xiaowei Chang contributed equally to this work.

https://doi.org/10.1016/j.bioactmat.2022.08.029
Received 15 April 2022; Received in revised form 23 August 2022; Accepted 29 August 2022

critical factors to address bone regenerative problems in DM. However, the bone defect area usually lacks MSCs, and the migration capacity of MSCs is significantly inhibited in DM [9,10]. Therefore, a proper strategy to effectively recruit MSCs is important. Stromal cell derived factor-1 (SDF-1) is a member of the CXC chemokine family that plays a critical role in the early migration of CXCR4 (CXC motif chemokine receptor type 4)-positive stem and progenitor cells to injury sites during the acute phase of bone repair [11,12]. Thus, the exogenous delivery of SDF-1 to the bone defect area might enhance the recruitment of bone marrow mesenchymal stem cells (BMSCs) under T2DM conditions. Meanwhile, disordered glucose metabolism in DM overproduced ROS, which makes it difficult for single MSCs treatment to play its role in the diabetic microenvironment [13,14]. Metformin is well known as the first-line antihyperglycemic agent, and has also been used to reduce the incidence of fracture in diabetic patients [15,16]. Many clinical experiments have revealed that the local use of metformin in periodontal pockets can achieve a certain degree of periodontal regeneration [17]. Moreover, it was reported that metformin could partially restore the damaged osteogenic potential of MSCs by eliminating ROS [18,19]. Therefore, the codelivery of SDF-1 and metformin in the defect area may open a window for improving periodontal bone regeneration in DM. However, the proper delivery order and period of SDF-1 and metformin to achieve optimal therapeutic efficacy is still a challenge.

Natural bone tissue regeneration is a multistage and well-orchestrated process consisting of MSC recruitment, angiogenesis and osteogenesis etc. [20], and each stage has a demand for a specific biological signal, which gives us an inspiration to emulate the natural healing cascade toward bone regeneration [21]. Although many studies have seen MSC recruitment and osteogenesis as two of the most important stages in the bone regeneration process, few of them pay attention to the cascade effect between them [7]. Based on the MSC "recruitment-osteogenesis" cascade of natural bone healing, rapid release of SDF-1 for MSC recruitment at the beginning and slow release of metformin for sustained ROS elimination and osteogenic promotion are required to achieve efficient periodontal bone regeneration in DM.

Polymeric hydrogels have been used as drug delivery systems in tissue engineering for years due to their similar structure to the natural extracellular matrix (ECM), high drug loading capacity and good biocompatibility, making them promising candidates for periodontal bone regeneration after loading with SDF-1 and metformin [22–24]. However, direct incorporation of these two drugs into polymeric hydrogels would cause fast corelease due to their porous structure and high water content. This process mismatches the natural bone regenerative procedures requesting SDF-1 and metformin at different time periods, which may cause low efficiency. Moreover, the complex periodontal structure also limits the application of conventional hydrogels via implantation.

Herein, an injetable hydrogel was fabricated using thermosensitive poly (D,L-lactide)-block-poly (ethylene glycol)-block-poly (D,L-lactide) (PDLLA-PEG-PDLLA) copolymer and mesoporous silica nanoparticles (MSNs), which performed sequential releases of SDF-1 and metformin fitting the natural bone healing cascade for diabetic bone regeneration. The PDLLA-PEG-PDLLA consists of both poly (DL-lactide) segments and polyethylene glycol segments (Fig. S1). In the fabrication process, metformin (Met) was first encapsulated in mesoporous silica nanoparticle (MSN) to form Met@MSN and then coassembled with PDLLA-PEG-PDLLA. The resulting thermosensitive assemblies served as hydrogel precursors after mixing with SDF-1, which switched to the PDLLA-PEG-PDLLA-Met@MSN-SDF-1 (PPP-MM-S) hydrogel once the ambient temperature was over 35 °C. Based on the different loading approaches, the hydrogel achieved relatively quick SDF-1 release for early rat BMSC (rBMSC) recruitment at first, followed by the sustained release of metformin from exposed MSNs along with the slow degradation of PDLLA-PEG-PDLLA, to scavenge the overproduced ROS under high glucose conditions. This synergistic therapy not only provided sufficient rBMSCs for bone regeneration, but also effectively reduced the ROS to reverse the inhibited osteogenic differentiation of rBMSCs, resulting in continuous regulation of the diabetic microenvironment and facilitation of osteogenesis, which realized precise manipulation over the MSC "recruitment-osteogenesis" cascade for diabetic bone regeneration (Scheme 1).

2. Materials and methods

2.1. Synthesis of triblock copolymer PDLLA-PEG-PDLLA

PEG_{1500} (4 g) was heated in vacuum at 100 °C for 1 h to eliminate trace amounts of water. After the flask was cooled to room temperature, D, L-lactide (8 g) and Sn $(Oct)_2$ (36 mg) were added. The reaction was carried out at 140 °C for 12 h under N_2 protection. Finally, the resulting PDLLA-PEG-PDLLA block copolymer was dissolved in ethanol (12 ml) and reprecipitated from the filtrate using excess pre-cold n-pentane (120 ml). The sediment was vacuum dried to constant weight at 45 °C.

2.2. Synthesis of MSNs

The pH value of deionized water (1000 ml) was adjusted to approximately 11 with ammonium hydroxide (52.8 ml, 25 to 28 wt % $NH_3{\cdot}H_2O$). The temperature was raised to 50 °C, and then, CTAB (1.12 g) was added. After the CTAB was completely dissolved, tetraethylorthosilicate (5.8 ml) was added dropwise with rapid stirring. After 2 h, the mixture was incubated overnight, centrifuged, and washed thoroughly with distilled water and ethanol. As-synthesized silica nanoparticles were dispersed in ethanol by sonication for 30 min, followed by the addition of 20 ml of a 1:1 mixture (v/v) of water and mesitylene. The mixture was placed in the autoclave and kept at 140 °C for 4 days without stirring. The resulting white powder was washed with ethanol and water five times each. Then, the surfactant templates were removed by extraction using acidic methanol (9 ml of HCl/400 ml of methanol, 36 h) at 70 °C, and then the MSNs were centrifuged, washed several times with ethanol, and dried under vacuum for 20 h.

2.3. Synthesis of Met@MSN

MSNs (20 mg) were added to deionized water (5 ml) and sonicated to disperse. Then, metformin (5 mg) was added to this mixture. After stirring for 24 h, the Met@MSN was centrifugalized, washed with deionized water three times, and freeze dried.

2.4. Preparation of PDLLA-PEG-PDLLA-Met@MSN-SDF-1 hydrogel

The as-synthesized Met@MSN (10 mg) was added to PDLLA-PEG-PDLLA (250 mg), and the mixture was stirred at rt for 10 min. Then, deionized water (0.9 ml) was added to this mixture. The Met@MSNs were coassembled with PDLLA-PEG-PDLLA in water to obtain PDLLA-PEG-PDLLA-Met@MSN nanocomplexes via hydrophilic-hydrophobic interactions. Finally, SDF-1 (0.1 ml, 6 μg/ml) was added to generate the precursor solution of the PDLLA-PEG-PDLLA-Met@MSN-SDF-1 hydrogel. As expected, the resulting nanocomplex solution could perform a sol-gel transition at 37 °C to form the PDLLA-PEG-PDLLA-Met@MSN-SDF-1 hydrogel.

2.5. Cell isolation and culture

Bone marrow was obtained from young male Sprague–Dawley (SD) rats (4–6 weeks old) by cutting off both ends of the femora. Cells were cultured in normal-glucose (NG) medium (α-MEM with 5.5 mM D-glucose; Gibco, Grand Island, USA) supplemented with 10% fetal bovine serum (FBS; Gemini, Woodland, USA), 100 U/mL penicillin, and 100 μg/mL streptomycin (Biosharp, Anhui, China) at 37 °C in a humidified CO_2 incubator. The medium was replaced every three days during culture. For all experiments, only rBMSCs at early passages (passages 3–5) were

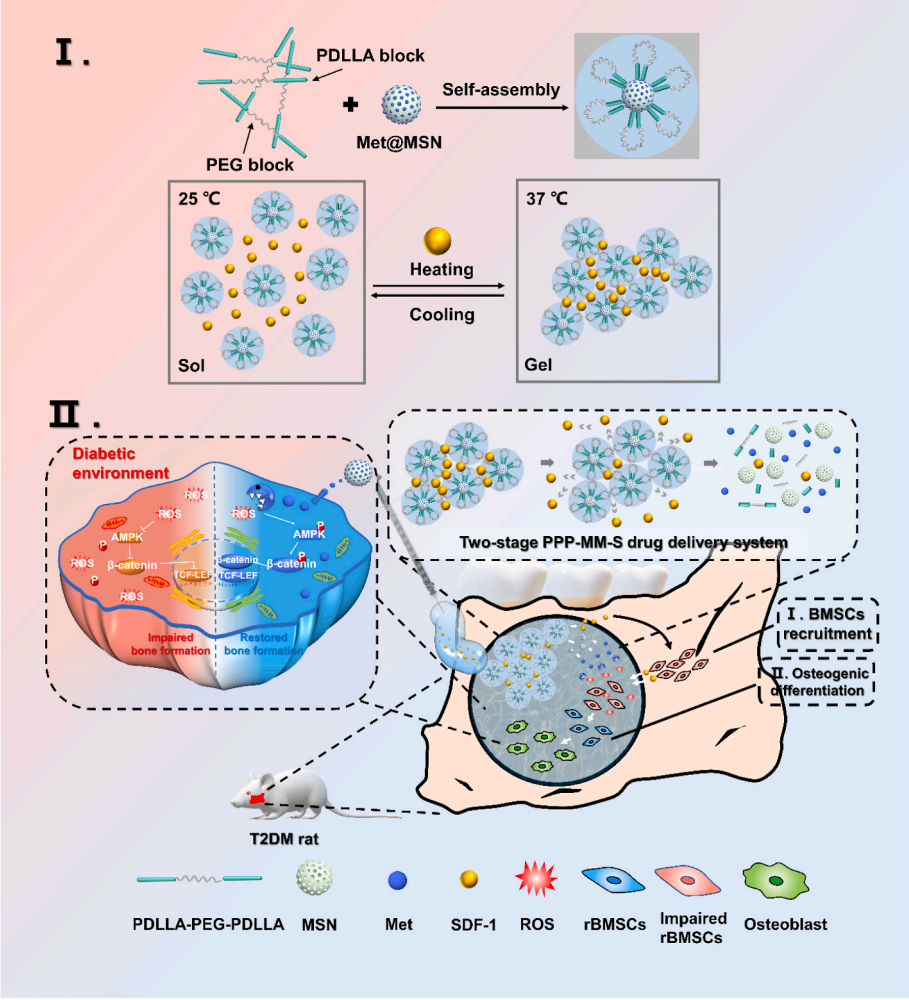

Scheme 1. Schematic diagram depicting the design principle of the bioinspired hydrogel emulating the cell "recruitment-osteogenesis" cascade for diabetic periodontal bone regeneration and the mechanism of metformin restoring bone homeostasis through the ROS/AMPK/β-catenin pathway under high-glucose conditions.

used in this study, and cells were harvested using a trypsin/EDTA solution (Biosharp, Anhui, China) and resuspended in fresh medium. The glucose concentration of the high-glucose (HG) medium was set at 44 mM according to a previous study [25], and the HG medium was prepared by the addition of D-glucose (38.5 mM, Solarbio, Beijing, China) to the NG medium. For osteogenic induction, the media were additionally supplemented with 50 μg/ml ascorbic acid 2-phosphate, 10 mM β-glycerophosphate, and 10 nM dexamethasone (Solarbio, Beijing, China).

2.6. Osteogenesis experiments

To investigate whether an HG environment affects the osteogenic differentiation of rBMSCs and the effect of metformin, rBMSCs were cultured in osteogenic medium and divided into 4 groups: 1) the normal-glucose (NG) group, the cells in which were cultured in normal-glucose (5.5 mM) medium; 2) the high-glucose (HG) group, the cells in which were cultured in HG (44 mM) medium; 3) the NG + Met group, the cells in which were cultured in NG medium treated with metformin (100 μM); or 4) the HG + Met group, the cells in which were cultured in HG medium supplemented with metformin. The medium was changed every three days.

To further investigate the osteogenic effect of our drug-delivery systems on rBMSCs under HG conditions, we set up 6 groups: A: the control group (NG), B: the untreated high glucose group (HG), C: the HG/PPP-M group, D: the HG/PPP-M-S group, E: the HG/PPP-MM group, and F: the HG/PPP-MM-S group. A 24-cell Transwell plate (pore size: 8 μm; Merck, Cambridge, USA) was used. The rBMSCs were seeded into the lower chambers at a density of 5×10^4 cells/well, and the hydrogels were placed in the upper chambers. The osteogenic induction medium in the lower chambers was replaced every three days, but the hydrogels in the upper chambers were not replaced for the entire osteogenic induction process to enable the sustained release of the drugs into the lower chambers.

2.7. Intracellular ROS measurement

The fluorescent probe H2DCFH-DA (Biosharp, Anhui, China) was used to test the level of ROS. Briefly, the cells were washed with PBS twice and incubated with H2DCFH-DA solution (10 μM) for 30 min in the dark. After rinsing with PBS three times, the cells were observed under a fluorescence microscope.

2.8. Alkaline phosphatase and alizarin red S staining

After 7 days of culture, ALP staining was performed with an ALP staining kit (Beyotime, Shanghai, China). Briefly, the samples were washed twice with phosphate-buffered saline (PBS), fixed with 4% paraformaldehyde (PFA, Solarbio, Beijing, China) for 30 min and washed twice with PBS again to remove the participating fixative. After that, the staining of the cells was conducted according to the instructions. After staining, the samples were observed, and images were

captured. After 21 days of culture, the rBMSCs were washed and fixed. Alizarin Red solution (Solarbio, Beijing, China) was added to the wells, and the plates were incubated for 30 min. After incubation, the samples were washed 3 times with deionized water, and the plates were observed and imaged.

2.9. Reverse transcriptase quantitative polymerase chain reaction (RT–qPCR)

After 7 and 14 days of culture, the rBMSCs were washed with PBS twice and harvested to extract total RNA with TRIzol reagent (Takara, Tokyo, Japan). Then, the iScript cDNA synthesis kit (Takara, Tokyo, Japan) was utilized to synthesize cDNA. RT–qPCR assays were performed to determine *runt-related transcription factor 2* (*Runx2*), *Sp7 transcription factor* (*Sp7*), and *collagen type I* (*Col1a1*) expressions in rBMSCs using SYBR-Green Premix Ex Taq (Takara) and a CFX96 Real-Time PCR Detection System (Bio–Rad Laboratories, Inc., Hercules, CA, USA). *β-Actin* was used as the internal control. The sequences of the primers used are listed in Table S1 in the Supporting Information.

2.10. Chemotactic effect of SDF-1 on rBMSCs under high glucose

A 24-cell Transwell system (pore size: 8 μm; Merck, USA) was used to evaluate the influence of SDF-1 on the migration ability of rBMSCs under HG conditions. The rBMSCs were starved for 3 h and loaded into the upper chamber of the Transwell system at a density of 1×10^5 cells/well. NG or HG culture media with or without SDF-1 (100 μg/L; Novoprotein, Suzhou, China) were placed in the lower chamber. After 24 h, migrated rBMSCs were fixed with 4% PFA (Solarbio) for 30 min and then stained with 0.2% crystal violet (Solarbio, Beijing, China). Migrated cells (on the bottom surface of the transwell) were visualized by microscopy. We selected six random visual fields per well for viewing, and the number of cells was quantified by counting. For the wound healing assay, cells were seeded in a 6-well plate. A wound was made in the center of each well by scratching with a 200 μl pipette tip. Then, the cells were cultured in the same groups as mentioned above. Scratch wounds were imaged using an inverted microscope (Nikon Corporation, Tokyo, Japan) at 0 and 24 h post-wounding, and the migration areas were measured using ImageJ software (National Institutes of Health, MD, USA).

2.11. Cytotoxicity assessment of the drug-delivery system

First, we detected the cytotoxicity of MSNs and the PPP hydrogel using the Cell Counting Kit-8 (CCK-8; Biosharp, Anhui, China) assay. Confluent rBMSCs were trypsinized, seeded in a 96-well plate at 2×10^3 cells/well and incubated for 24 h. Then, the medium was replaced with fresh medium or medium with solutions of MSNs, PPP hydrogel, or PPP-M hydrogel. After incubation for 1 and 3 days, the absorbance at 450 nm was read with a microplate reader (PerkinElmer, Waltham, USA).

To further investigate the effect of the hydrogels on the proliferation of rBMSCs, we established 6 groups: A: the control group (NG), B: the untreated HG group, C: the HG/PPP-M group, D: the HG/PPP-M-S group, E: the HG/PPP-MM group, and F: the HG/PPP-MM-S group. Cells were seeded in 96-well plates and cocultured with or without the extracts of the drug delivery systems for 1, 3, 5, and 7 days. At each timepoint, cell viability was detected by CCK-8 assay. On the 1st, 4th and 7th days, cells were treated with a calcein-AM/PI (live/dead) double staining kit (Dojindo, Tokyo, Japan), and images were captured under a laser confocal scanning microscope (LCSM; Leica SP8, Heidelberg, Germany).

Hemolysis analysis was carried out to further evaluate the biocompatibility of the PPP-M and PPP-MM-S hydrogels. Briefly, fresh blood was obtained from the hearts of SD rats and used to investigate the hemolytic activity of hydrogel. Red blood cells were separated from the plasma and hemoglobin release was analyzed at 576 nm. Saline solution and double distilled water were used as the negative and positive control groups, respectively.

2.12. Western blot analysis

Total protein was isolated from rBMSCs using RIPA lysis buffer (Beyotime) with 1 mM phenylmethanesulfonyl fluoride (PMSF; Beyotime). Nucleoproteins were isolated according to the instructions of a Nuclear and Cytoplasmic Protein Extraction Kit (Beyotime). Then, the protein concentrations were quantified using a BCA kit (Beyotime). Fifteen microliters of each protein sample was separated via sodium dodecyl sulfate–polyacrylamide gel electrophoresis (SDS–PAGE; Beyotime), and the proteins were then transferred onto a polyvinylidene difluoride (PVDF) membrane (Bio–Rad). After blocking with 5% BSA for 2 h, the membranes were incubated with primary antibodies overnight at 4 °C, followed by incubation with the corresponding secondary antibodies for 2 h after washing three times with TBST. Thereafter, the protein bands were detected with PLUS electrochemiluminescence reagent (Bio–Rad). Finally, the intensity of the protein bands was quantified with ImageJ software (National Institutes of Health, Bethesda, MD, USA) and normalized to the internal control: β-actin for total protein and Lamin B1 for nucleoproteins.

2.13. In vivo degradation and toxicity of the drug-delivery system

To evaluate the *in vivo* degradation performance of the drug-delivery system, the SD rats were shaved in the back and the PPP-M and PPP-MM-S hydrogels were implanted subcutaneously [14], and rats that were shaved in the same way but weren't implanted with hydrogel were used as the control group. The size of the subcutaneous hydrogels was observed within a month and photos were taken. Four weeks after the implantation, the skin in the back was incised to evaluate the degradation situation of the implanted hydrogel.

To detect the bio-toxicity of the hydrogel during the treatment, the hydrogel was implanted to periodontal defect of the SD rat. Their heart, liver, spleen, lung and kidney tissues were harvested 4 and 8 weeks after the operation. The samples were sectioned for H&E staining. Moreover, 200 μl hydrogels were implanted subcutaneously in the back of SD rats. The skin and subcutaneous tissue of the implantation area was harvested and sectioned for H&E staining to detect the toxicity of the hydrogels after 4 weeks [13].

2.14. Induction of T2DM in rats

The animal experiments were conducted according to experimental animal ethics and welfare guidelines approved by the ethics committee of the College of Stomatology, Chongqing Medical University (permit number: CQHS-REC-2020 (LSNo. 76)). T2DM rats were prepared as previously described [26,27]. 4-week-old Male Sprague Dawley (SD) rats (100–150 g) were fed with high fat diet (HFD) for 4 weeks. After 4 weeks, rats were injected intraperitoneally with streptozotocin (STZ) dissolved in sodium citrate buffer (pH 4.5, prepared immediately before use) at a dose of 35 mg/kg. One week later, the rats were fasted overnight, and their fasting blood glucose were measured in the next morning. The rats with fasting blood glucose higher than 11.1 mmol/L, combined with symptoms like polyuria, polydipsia and weight loss, were considered diabetic and included in the experimental group. For the rats that weren't diagnosed with diabetes, they would be injected intraperitoneally with STZ again at a dose of 35 mg/kg when their fasting blood glucose returned to the normal level (≤7.0 mmol/L). The age-matched SD rats which were fed regular chow for 4 weeks and injected with vehicle were used as the control group. The T2DM rats were randomly divided into 5 groups: 1) the untreated T2DM group, 2) the T2DM/PPP-M group, 3) the T2DM/PPP-M-S group, 4) the T2DM/PPP-MM group, and 5) the T2DM/PPP-MM-S group.

2.15. Periodontal bone defect model preparation and regeneration in vivo

Mandibular periodontal bone defects were created as previously reported with modifications [28]. After the rats had been anesthetized, the fur surrounding the surgical area was removed, and the skin was disinfected. A 1.5-cm incision was made along the inferior border of the mandible to expose the masseter muscle. Following dissection of the masseter muscle and localization of the buccal plate, a ring drill was used to initiate access to the buccal root, followed by the use of a No. 1/2 bur to complete the osteotomy to create a standard round defect with a size of 3 × 3 mm. Then, the defects were loaded with sterilized hydrogels or left untreated, and the muscle and skin over the surgical site were repositioned and sutured. After the operation, all the rats were injected with analgesia for 3 days and fed soft food for 7 days. For the assessment of periodontal bone regeneration, the other rats were sacrificed 4 or 8 weeks after the operation. Their mandibles were harvested and fixed in 4% PFA for subsequent histological examination. The regenerative efficacies of the hydrogels were assessed by microcomputed tomography (micro-CT) scanning. The samples were decalcified with 10% EDTA and sectioned for H&E and Masson trichrome staining.

2.16. rBMSC recruitment in vivo

To evaluate rBMSC recruitment *in vivo*, the rBMSCs were trypsinized and centrifuged. Then, the cells were resuspended gently in prewarmed PBS containing the CFSE probe (Invitrogen, California, USA) and incubated at 37 °C for 15 min. After that, the cells were incubated for another 30 min and observed under a fluorescence microscope. After the preparation of periodontal bone defects in rats, rBMSCs labeled with CFSE were injected into the circulation of rats through the caudal vein (1×10^6 cells per rat). One week postoperation, the mandibles of the rats were harvested. Then, the samples were fixed, embedded in resin and sectioned using a hard tissue slicing technique. The sections were observed under a confocal fluorescence microscope for CFSE-labeled rBMSCs that migrated to the periodontal defect area.

2.17. Statistical analysis

The data are presented as the mean ± standard deviation. One-way analysis of variance (ANOVA) was used to analyze the significance of differences between samples. For all tests, the level of significance was set to $p < 0.05$, $p < 0.01$, $p < 0.001$ and $p < 0.0001$. All the data were statistically analyzed with GraphPad Prism 9.0 (GraphPad Software Inc., San Diego, CA, USA).

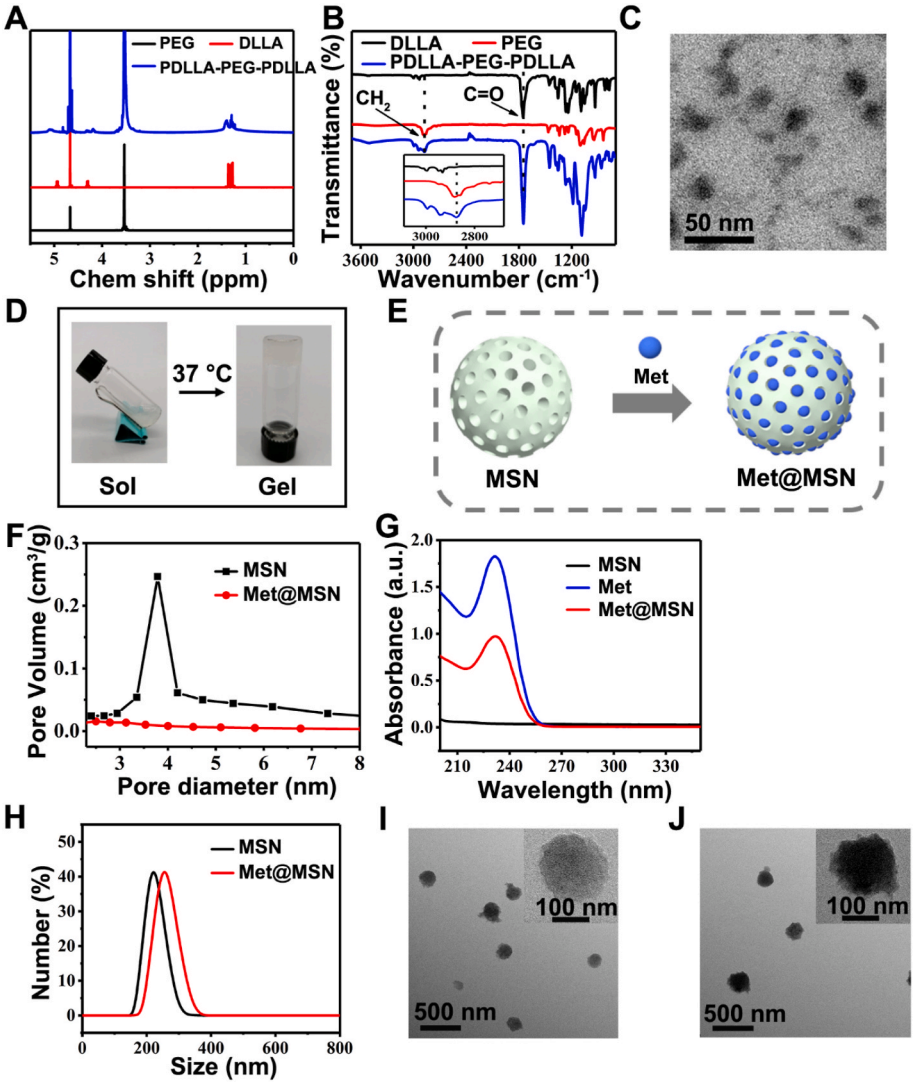

Fig. 1. Synthesis and characterization of PDLLA-PEG-PDLLA and Met@MSN. A) ^{1}H nuclear magnetic resonance (NMR) and B) Fourier transform infrared (FTIR) spectra of PEG, DLLA and PDLLA-PEG-PDLLA. C) TEM image of PDLLA-PEG-PDLLA micelles. D) Gel-sol transition of PDLLA-PEG-PDLLA hydrogel at 37 °C. E) Synthesis scheme of Met@MSN. F) UV–Vis spectra of MSN, metformin and Met@MSN. G) Pore size distribution and H) hydrodynamic size distribution of the MSN and Met@MSN. I) TEM image of MSN. J) TEM image of Met@MSN.

3. Results and discussion

3.1. Preparation and characterization of the PPP-MM-S hydrogel

To prepare the PPP-MM-S hydrogel, the triblock copolymer PDLLA-PEG-PDLLA (PPP) was first synthesized by ring-opening polymerization of D,L-lactide (DLLA) using PEG as the initiator and stannous octoate as the catalyst [29]. The as-synthesized polymer was investigated by nuclear magnetic resonance (NMR) spectrometry (Fig. 1A), which presented characteristic peaks of CH_2 (δ 3.53) from PEG as well as CH_3 (δ 1.41–1.22) and CH_2 (δ 5.11–5.03, δ 4.33–4.12) from PDLLA, indicating the successful formation of PDLLA-PEG-PDLLA. Further information was provided by the Fourier transform infrared (FTIR) spectra (Fig. 1B), which presented characteristic vibrations of C═O (1752 cm^{-1}) from PDLLA and CH_2 (2890 cm^{-1}) from PEG. The resulting PDLLA-PEG-PDLLA was able to assemble in water to form micelles (Fig. 1C), which would further switch to hydrogel under body temperature as expected (Fig. 1D). The frame of hydrogel was further dyed by fluorescent dye (rhodamine) and then measured by fluorescence microscopy. As can be seen from Fig. S2, the red frame of the hydrogel was separated by black pores, which were vacancy unable to be labeled by rhodamine, indicating that our hydrogel had typical porous structure as expected.

After obtaining the PDLLA-PEG-PDLLA and demonstrating its gelation ability, mesoporous silica nanoparticles, the other important ingredient of the PPP-MM-S hydrogel, were synthesized by the classical CTAB-templated and base-catalyzed sol-gel method. The pores of MSNs were further loaded by metformin (Met) to form Met@MSNs (Fig. 1E). The loading process was investigated by Brunauer–Emmett–Teller (BET) calculations and UV–Vis spectroscopy, which presented a dramatic decrease in pore volume down to 0 and the appearance of a new signal of metformin, indicating that the pores of MSNs were completely filled by metformin (Fig. 1F and G). Although the hydrodynamic size of Met@MSN was slightly enhanced compared with MSN due to the drug loading (Fig. 1H), it still maintained the spherical structure, in which the blockage of pores could be clearly observed (Fig. 1I and J). The high resolution transmission electron microscopy images of MSN before and after loading metformin were presented in Fig. S3. As can be seen from this figure, the MSN had obvious mesoporous structure, which clearly disappeared after metformin loading. This phenomenon means that the metformin molecules are able to enter and fill the pores of MSN, resulting in the significant decrease of the pore size from 4 nm to nearly 0 nm after metformin loading. More details of the structure of Met@MSN were provided by the mapping model of EDX. As can be seen from Fig. S4, beside the characteristic elements of Si and O from MSN, the obvious signal of N and C from metformin was also observed, which exactly co-located with the spherical MSN, indicating the successful encapsulation of metformin in the pores of MSN as expected.

The as-synthesized Met@MSNs were further coassembled with PDLLA-PEG-PDLLA in water to obtain PDLLA-PEG-PDLLA-Met@MSN (PPP-MM) nanocomplexes via hydrophilic-hydrophobic interactions. Then, SDF-1 was added to generate the precursor solution of the PPP-MM-S hydrogel. In order to find the proper quantity of Met@MSN for optimal performance of the gel, different amounts of Met@MSN (0 mg, 5 mg, 10 mg, 15 mg and 20 mg) were assembled with PDLLA-PEG-PDLLA (250 mg) to form the hydrogel (1 ml). The mechanical and degradation properties of these hydrogels were measured by rheological analysis (Fig. S5) and mass change against incubation time (Fig. S6). As shown in these figures, no obvious changes of mechanical and degradation properties of the hydrogel were observed until the concentration of Met@MSN was over 10 mg/ml. Therefore, in order to achieve the maximum drug loading while maintaining the best mechanical and degradation properties, the concentration of Met@MSN at 10 mg/ml was used to prepare the hydrogel. To calculate the drug loading percentage of metformin in the hydrogel, the loading percentage of metformin in MSNs was measured at first using UV–Vis spectrum, which was 18 wt% determined by typical absorption of metformin at 232 nm (Fig. S7). Considering the mass ratio of PDLLA-PEG-PDLLLA, Met@MSN and SDF-1 at 250 mg:10 mg: 0.6 μg was selected to prepare the hydrogel, in which all the agents were completely used without wasting, the loading percentage of metformin and SDF-1 in the hydrogel were set at 38 mg/g and 2 μg/g, respectively. The PPP-MM nanocomplex was investigated by TEM and dynamic light scattering (DLS), which showed a spherical structure with an additional organic layer and enhanced hydrodynamic size compared with Met@MSN (Fig. 2A and B), indicating the assembly of PDLLA-PEG-PDLLA on the surface of Met@MSN.

As expected, the resulting nanocomplex solution could also perform sol-gel transition at 37 °C to form PPP-MM-S hydrogel **(**Fig. 2C**),** and the cargos (Met@MSN and SDF-1) were both uniformly distributed in the whole hydrogel (Fig. 2D). As shown in Fig. S8, the mechanical property of the hydrogel was further measured by rheological analysis, in which the G′ was always larger than G″ under different conditions, indicating the typical rheological data of hydrogel. The release of SDF-1 and Met@MSN from the hydrogel was driven by diffusion and degradation, respectively (Fig. 2E). The rapid molecular diffusion through the hydrogel network and slow degradation of the hydrogel up to one month under a simulated physiological state (Fig. 2F) led to fast SDF-1 release with approximately 80% drug escape in 2 weeks and sustained metformin release ending at day 30 (Fig. 2G and H). The concentrations of SDF-1 and metformin that actually released from the hydrogel were also presented in Fig. S9. As can be seen from these figures, the rapid release of SDF-1 results in a drug concentration of 0.5 μg/ml close to the maximum value in the first 2 weeks. In contrast, the release of metformin maintained 4 weeks ending up with a drug concentration of 0.9 mg/ml at day 30. Fast SDF-1 release in the first two weeks was employed to recruit BMSCs meeting the demand of early-stage bone regeneration [11,12], while the sustained release of metformin was responsible for remodeling the diabetic microenvironment and further facilitating osteogenesis [30]. To clearly demonstrate these two processes, we showed the fluorescence spectra of the hydrogel before and after release (Fig. 2H). We used four groups of drug-delivery systems containing either SDF-1 or metformin to compare their effects in the following experiments (Table 1).

3.2. Metformin induced rBMSC osteogenesis under high-glucose conditions in vitro

Hyperglycemia is one of the most important contributors to dysfunction in T2DM [31–33]. ROS are overproduced in diabetes and have a negative effect on osteogenesis [34]. The rBMSCs were therefore cultured in a high glucose (HG) environment *in vitro* to investigate whether the production of ROS and their osteogenic process were influenced. rBMSCs cultured under normal glucose (NG) conditions were used for comparison. Metformin was added to investigate its influence on osteogenesis (Fig. 3A). As shown in Fig. 3B and G, excessive ROS (green signal) were produced in rBMSCs in a HG environment. Notably, metformin significantly eliminated ROS in rBMSCs. After culture for 7 days, ALP staining showed lighter staining in the HG group than in the NG group (Fig. 3C). However, the HG + OI + Met group displayed darker staining than the HG + OI group and it was comparable to that of NG + OI group (Fig. 3C). The results of Alizarin Red staining showed the same trends (Fig. 3D). The above results indicated that the HG environment, which is an important contributor to T2DM-related disorders, probably plays a significant role in osteogenic impairment under diabetic conditions [35]. Notably, metformin could alleviate the negative effect of HG on bone metabolic homeostasis to a great extent. In addition, it was interesting to find that NG + OI + Met group exhibited darker ALP staining and lighter alizarin red staining than NG + OI group (Fig. 3C and D), indicating that metformin might not have a definitely positive influence on the osteogenic differentiation of rBMSCs under NG conditions, which was consistent with the results of the previous study [36].

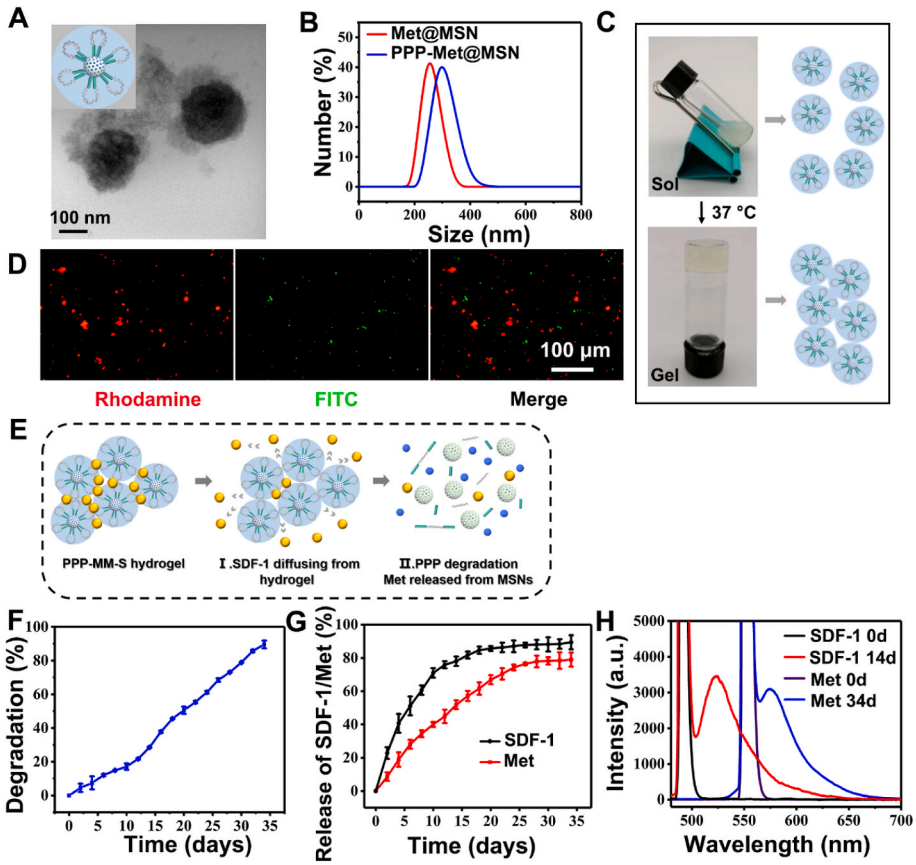

Fig. 2. Construction and characterization of PDLLA-PEG-PDLLA-Met@MSN-SDF-1 hydrogel. A) TEM image of PDLLA-PEG-PDLLA-Met@MSN nanocomplex. B) The hydrodynamic size distribution of Met@MSN and PDLLA-PEG-PDLLA-Met@MSN nanocomolexes. C) Gel-sol transition of the PDLLA-PEG-PDLLA-Met@MSN-SDF-1 hydrogel. D) Fluorescence images of the PDLLA-PEG-PDLLA-Met@MSN-SDF-1 hydrogel, in which metformin was labeled with red fluorescence dye (rhodamine) and SDF-1 was labeled with green fluorescence dye (FITC). E) Cargo release schematic of the hydrogel. F) Degradation ratio and G) release profiles of the PDLLA-PEG-PDLLA-Met@MSN-SDF-1 hydrogel. H) Fluorescence spectra of solutions before and after 14 days of FITC-SDF-1 release and 34 days of rhodamine-metformin release.

Table 1
The groups of drug delivery systems.

	PPP-M	PPP-M-S	PPP-MM	PPP-MM-S
SDF-1	–	+	–	+
Metformin	–	–	+	+

3.3. SDF-1 induced rBMSC migration under HG conditions in vitro

For *in situ* bone regeneration, cell recruitment to the defect area is the critical first step [37–39]. However, previous studies have revealed that cell migration is negatively impacted in diabetes [9,10]. Herein, transwell migration assays and cell scratch tests were performed to assess the migration ability of rBMSCs under HG conditions and the influence of SDF-1 on this process. As shown in Fig. 3E and H, the number of migrated rBMSCs in the HG group was significantly decreased compared to that in the NG group. The HG + SDF-1 group exhibited obviously more migrated rBMSCs than the HG group, which was even comparable to that of the NG group. The NG + SDF-1 group also showed more migrated cells than the NG group. The scratch test displayed similar results (Fig. 3F, I). After 24 h, the HG group showed an obviously decreased migration areas than the NG group, while the HG + SDF-1 and NG + SDF-1 groups displayed significantly higher migration area than the HG and NG groups, respectively. The migration rate of HG + SDF-1 group was comparable to that of the NG group. These results suggested that the HG environment exerted a negative impact on rBMSC migration capacity and that SDF-1 could effectively alleviate this trend, even to a nearly normal level. Cell recruitment occurs in the initial phase of natural bone repair and plays a critical role in the whole process [12]. Previous studies have demonstrated that SDF-1 and its receptor CXCR4 play an important role in mobilizing MSCs [40]. Our results revealed that it could partially reverse the inhibition of the HG environment on cell migration and thus held great potential for cell recruitment in diabetic bone regeneration [41–43].

3.4. Metformin restored the impaired osteogenic differentiation under HG conditions through the ROS/AMPK/β-catenin pathway

Considerable evidence has demonstrated that MSCs deteriorate and exhibit reduced osteogenic capability under diabetic conditions [44]. In this study, the results showed that the HG environment significantly increased the production of ROS and negatively impacted the osteogenesis of rBMSCs, and metformin partially reversed these trends. However, the specific mechanism of T2DM-induced BMSC dysfunction and how metformin works in this process are still not fully understood. Herein, we further explored the mechanism by which ROS and metformin affect bone homeostasis under HG conditions.

Emerging evidence suggests that AMPK regulates cell differentiation in addition to its role in metabolic processes [45], and its activation might be linked to β-catenin stability [46]. The results of the Western blot assay (Fig. 4B) showed that the level of p-AMPK (the activated form of AMPK) was decreased under HG conditions and that metformin could partially reverse this decrease. Activation of the Wnt/β-catenin pathway in preadipocytes was reported to inhibit adipogenesis by keeping the preadipocytes in an undifferentiated state and promote osteogenesis by upregulating the expression of the *Runx2* gene [47,48]. As shown in Fig. 4B, HG conditions downregulated the expression of β-catenin and p-β-catenin (at Ser552). Phosphorylation of β-catenin at Ser552 facilitates its stability and accumulation in the nucleus. As shown in Fig. 4B, the levels of β-catenin and p-β-catenin in the nucleus were also decreased under HG conditions, which would downregulate the expression of downstream osteogenic factors, leading to the inhibition of osteogenic differentiation [49]. Significantly, metformin upregulated the level of β-catenin and p-β-catenin in the nucleus (Fig. 4C). In

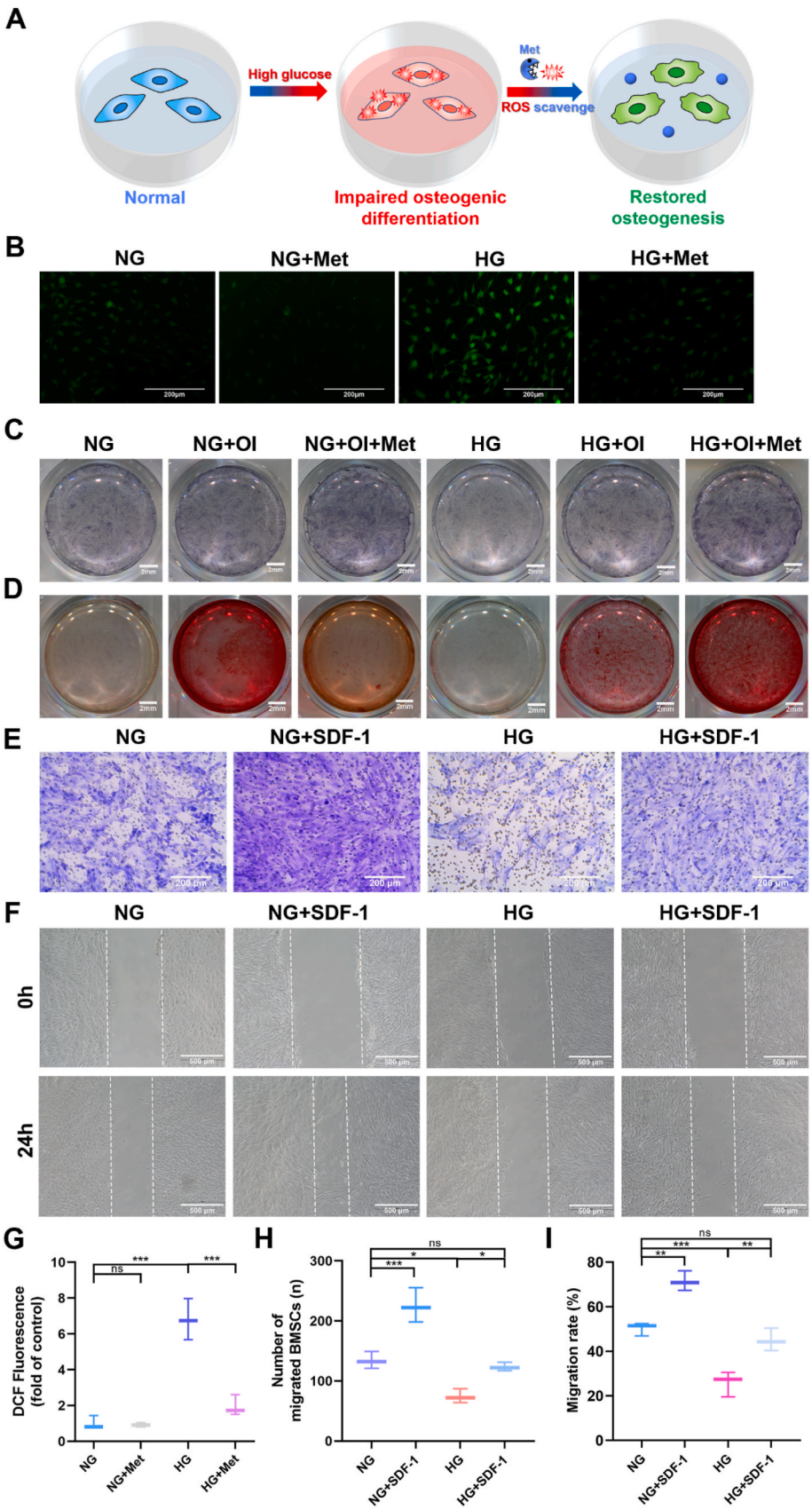

Fig. 3. The effect of metformin and SDF-1 on ROS overproduction, osteogenesis and migration capacity under high glucose conditions. A) Schematic diagram of metformin scavenging ROS and restoring cell osteogenesis under high glucose conditions. B) Representative fluorescent images of the intracellular ROS in rBMSCs cultured in normal glucose (NG), high glucose (HG) and HG + metformin (Met) groups and G) their quantitative analysis. C) ALP and D) alizarin red staining images of rBMSCs in the NG (normal glucose, complete medium), NG + OI (normal glucose, osteogenic inductive medium), NG + OI + Met (normal glucose, osteogenic inductive medium with metformin), HG (high glucose, complete medium), HG + OI (high glucose, osteogenic inductive medium) and HG + OI + Met (high glucose, osteogenic inductive medium with metformin) groups. E) Optical images of BMSCs recruited by SDF-1 in NG or HG using a transwell migration assay and H) the quantification of migrated rBMSC numbers. F) Optical images of wound healing assays and I) their quantitative analysis. Error bar represents the mean ± SD (n = 3); *, $p < 0.05$; **, $p < 0.01$, ***, $p < 0.001$; ns means not significant.

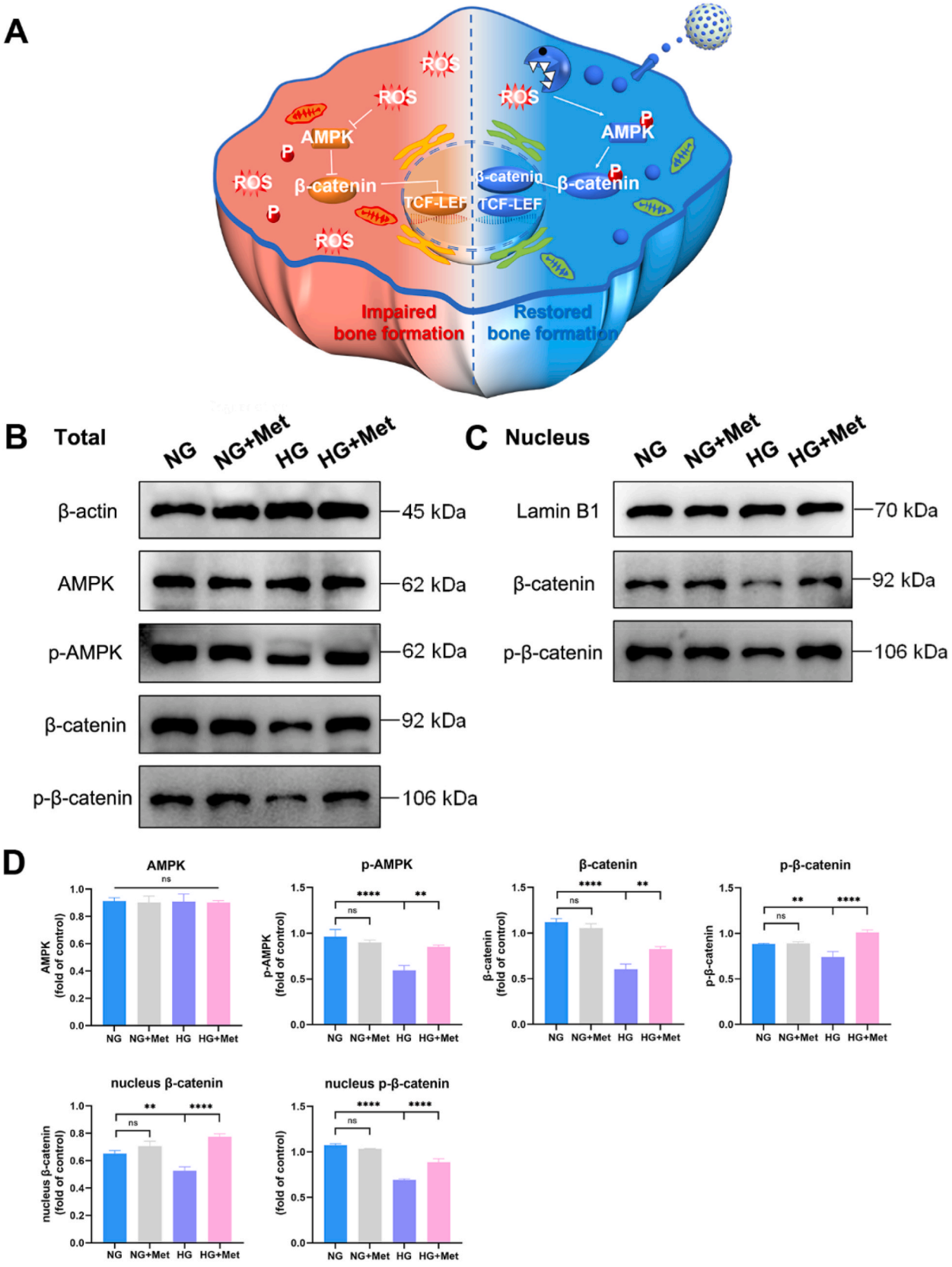

Fig. 4. Metformin promoted rBMSC osteogenesis under HG conditions through the ROS/AMPK/β-catenin pathway. A) Schematic image of metformin restoring cell bone metabolic homeostasis through the ROS/AMPK/β-catenin pathway under high glucose conditions. B) Western blot and C) quantitative analysis of AMPK, p-AMPK, β-catenin and p-β-catenin total or nuclear protein expression in NG (normal glucose), NG + Met (normal glucose, metformin treatment), HG (high glucose), HG + Met (high glucose, metformin treatment). Error bar represents the mean ± SD (n = 3); **, $p < 0.01$, ****, $p < 0.0001$; ns means not significant.

summary, our results indicated that metformin restored impaired osteogenesis through the elimination of excessive ROS produced under HG conditions, and it subsequently reactivated the inhibited AMPK/β-catenin pathway. Consequently, more β-catenin accumulated in the nucleus and it upregulated the expression of downstream osteogenic factors, restoring the inhibited osteogenic differentiation of rBMSCs under high glucose conditions (Fig. 4A). It's interesting to find that no obvious difference existed in p-AMPK, β-catenin and p-β-catenin expressions between the NG and the NG + Met groups, suggesting that metformin couldn't activate the AMPK/β-catenin pathway in normal glucose. It is consistent with the results of ALP and Alizarin Red staining that metformin might not be able to enhance the osteogenesis of rBMSCs under normal glucose conditions. Therefore, metformin could continuously scavenge overproduced ROS, and remodel the diabetic microenvironment to promote bone regeneration.

3.5. Cytotoxicity assessment of the drug-delivery system in vitro

It is essential that materials used in drug-delivery and regeneration engineering applications are biocompatible since toxic materials will be cleared by macrophages prior to their intended function [50]. To assess the cytotoxicity of the PPP hydrogel and MSNs, the CCK-8 assay was utilized to evaluate the survival and proliferation of BMSCs. As shown in Fig. 5A, no significant difference in cell viability was observed between the four groups after coculture for 1 and 3 days, indicating that both PPP and MSNs had good biocompatibility.

Cell proliferation under HG conditions was further investigated with or without the drug-delivery systems. As shown in Fig. 5B, no significant difference was observed between the NG and HG groups, indicating that an HG environment did not have a significant impact on cell proliferation. The viability of rBMSCs in all groups increased normally over time, suggesting that our drug-delivery systems had good biocompatibility. Moreover, the PPP-M-S group exhibited slightly higher cell viability than the other groups, while the PPP-MM and PPP-MM-S groups exhibited cell viability comparable to that of the PPP-M. This might be explained by the fact that SDF-1 could promote cell proliferation to some extent, and metformin facilitated the osteogenic differentiation of rBMSCs, which to some extent slowed cell proliferation [51].

A calcein-AM/PI (live/dead) kit was used to further evaluate the viability of rBMSCs cultured with the drug delivery systems for 1, 4 and 7 days. As shown in Fig. 5C, many living cells (colored green) and rare dead cells (colored red) were observed in all groups. Consistent with the CCK-8 assay results reported above, the number of live rBMSCs increased over time in all groups, and no significant difference in the number of live or dead cells was observed between the control and experimental groups. Additionally, the groups treated with SDF-1 exhibited slightly more living cells.

The blood compatibility of the biomaterial is essential for its biomedical application. As shown in Fig. S10, after 2 h co-incubation with rat red blood cells, the hydrogel groups displayed no apparent hemolysis.

In summary, the results indicated that HG conditions did not exert an obvious influence on cell viability, and our drug-delivery systems exhibited good cytocompatibility and blood compatibility. The hydrogel loaded with SDF-1 could slightly facilitate cell proliferation, while the hydrogel loaded with metformin did not exhibit a promotive effect on cell proliferation, probably because they facilitated the osteogenic differentiation of rBMSCs [51].

3.6. The PPP-MM-S system induced rBMSC osteogenic differentiation under HG conditions in vitro

To assess the osteoinductive capacity of the drug-delivery systems under HG conditions, we conducted RT–qPCR assays to detect the expression of osteogenic gene markers, including *Runx2*, *Sp7*, and *Col1a1*. The composite hydrogels were placed in the upper chamber of the transwell to simulate their constant drug-delivery effect *in vitro* (Fig. 4D). *Runx2* and *Sp7* are critical transcription factors in osteogenesis [52,53], and *Col1a1* plays an important role throughout the osteogenesis process [54]. As shown in Fig. 4E and F, HG conditions significantly inhibited the expression of *Runx2*, *Sp7* and *Col1a1* in rBMSCs, while the PPP-MM and PPP-MM-S groups showed significant reversal of the inhibitory effects of an HG environment. Moreover, the rBMSCs in the PPP-M-S group exhibited low expression levels of *Runx2*, *Sp7* and *Col1a1* on both the 7th and 14th days, comparable to those of PPP-M. These results indicated that our PPP-MM-S system could effectively restore the impaired osteogenic differentiation of rBMSCs under HG conditions. Additionally, PPP-M-S did not show an osteoinductive capacity under HG conditions, which was consistent with the results of cell proliferation experiments showing that PPP-M-S could promote the proliferation of rBMSCs. The difference between the PPP-MM and PPP-MM-S groups could be explained by the initial release of SDF-1 from the hydrogel facilitating the early proliferation of rBMSCs, and thus more cells were induced under the sustained influence of metformin [55]. These results preliminarily demonstrated the osteoinductive capacity of the PPP-MM-S hydrogel under HG conditions, which required further verification in the internal environment of T2DM rats.

3.7. In vivo degradation and toxicity of the drug-delivery system

As shown in Fig. S11A, the hydrogel implanted subcutaneously in the back of SD rats gradually degraded within 4 weeks. In Fig. S11B, both PPP-M and PPP-MM-S hydrogels could hardly be observed subcutaneously after 4-week degradation. The results suggested that the hydrogel could gradually degrade *in vivo* in 4 weeks, which was basically consistent with the results of their degradation performance *in vitro*.

As for the bio-toxicity of the drug-delivery system *in vivo*, as shown in Fig. S12A, compared with the control group, the results of viscera tissue H&E staining sections displayed the implantation of the hydrogels did not cause obvious organ damage or pathological change in major organs. Moreover, as shown in Fig. S12B, the implantation of the hydrogels caused little infiltration of immune cells in subcutaneous tissues and little inflammatory reaction was observed. In summary, the drug-delivery system could gradually degrade in 4 weeks, and it had little toxicity *in vivo*.

3.8. rBMSC recruitment in vivo

Following encouraging results from *in vitro* experiments, we further investigated the cell recruitment and osteogenesis effect of the PPP-MM-S hydrogel in a periodontal bone defect model of T2DM rats. A T2DM SD rat model was developed with a high-fat diet and streptozotocin (STZ) injection (Fig. 6A and B).

To assess the cell recruitment capacity, the rBMSCs were trypsinized and incubated with a CFSE probe. After 15 min, the cells labeled with CFSE showed bright green light (Fig. 6C). After the operation of the periodontal bone defect model in rats, the rBMSCs labeled with CFSE were injected into the circulation of rats. One week postoperation, the mandibles of the rats were harvested and sectioned to observe the injected CFSE-labeled rBMSCs that had migrated to the periodontal defect area. As shown in Fig. 6D, the control group exhibited some green light of migrated rBMSCs, suggesting that some cells had been recruited to the periodontal defect area by an endogenous recruiting effect. However, much weaker green light was found in the T2DM and PPP-M groups (Fig. 6D), probably because the endogenous recruiting effect was impaired in T2DM [9,10]. The PPP-M-S and PPP-MM-S groups exhibited significantly more green light than the other groups, indicating that the burst release of SDF-1 through diffusion effectively facilitated the migration of rBMSCs to the defect area [38]. In summary, the initially released SDF-1 emulated the early cell recruitment signal of the natural bone healing cascade and effectively facilitated cell migration to the defect area under diabetic conditions, which would lay a solid

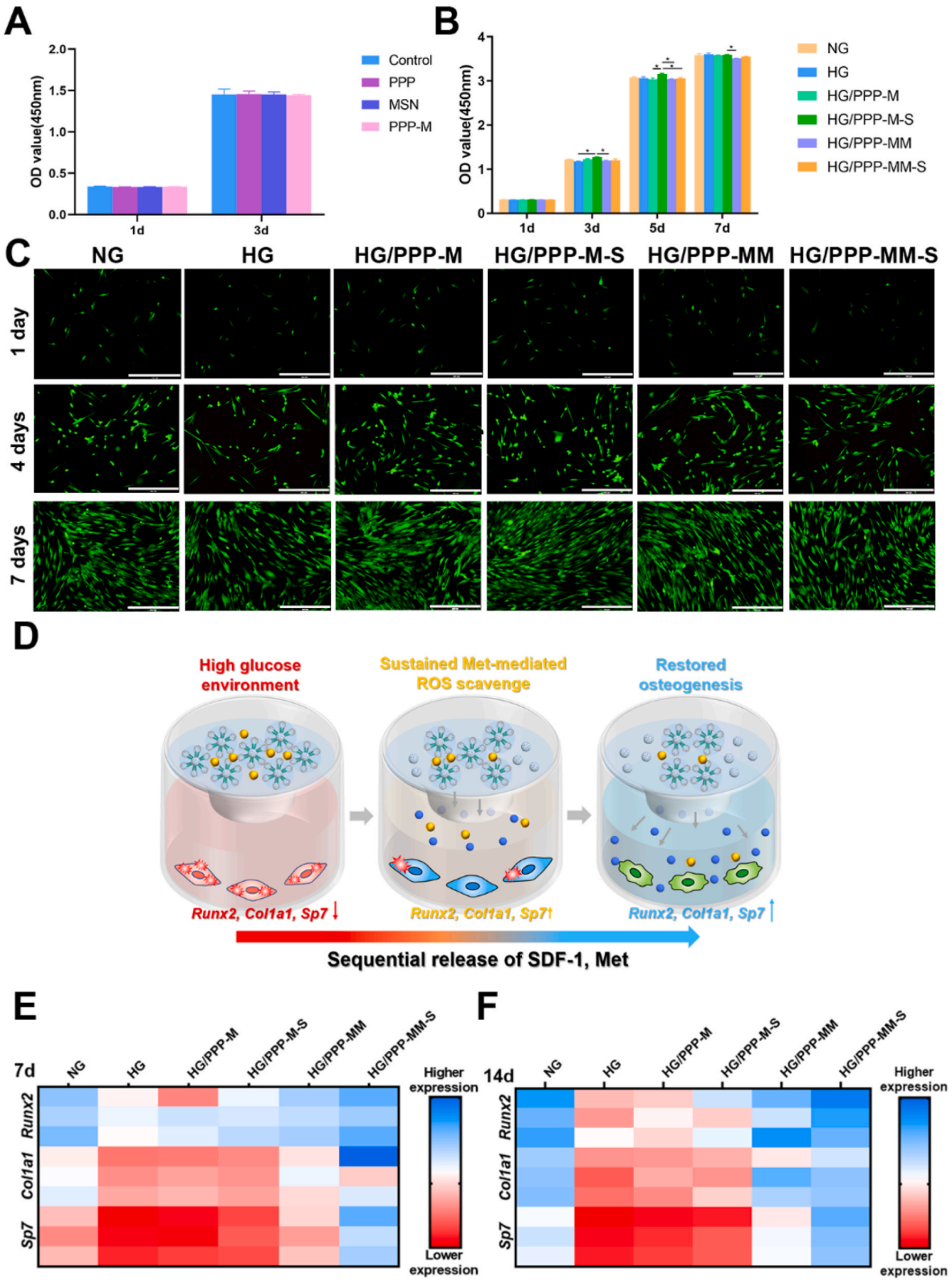

Fig. 5. ***In vitro*** **cytotoxicity assessment of the drug-delivery systems and its osteoinductivity in high glucose.** A) CCK-8 viability assay of rBMSCs cocultured with PPP, MSNs or both after culturing for 1 and 3 days. B) CCK-8 viability assay of rBMSCs cultured under normal glucose or high glucose conditions with the intervention of PPP-M, PPP-M-S, PPP-MM or PPP-MM-S hydrogel after culturing for 1, 3, 5 and 7 days. C) Live/dead cell staining images of rBMSCs cultured under normal glucose or high glucose conditions with the intervention of PPP-M, PPP-M-S, PPP-MM or PPP-MM-S hydrogel after culturing for 1, 4 and 7 days. Live cells were stained green, and dead cells were stained red. Scale bar: 400 μm. D) Schematic diagram of the PPP-MM-S hydrogel releasing SDF-1 and metformin from the upper chamber to the lower chamber scavenging ROS and restoring cell osteogenesis under high glucose conditions. E) Heatmap of relative gene expressions in rBMSCs incubated with hydrogels under different conditions (n = 3). Error bar represents the mean ± SD (n = 3); *, $p < 0.05$.

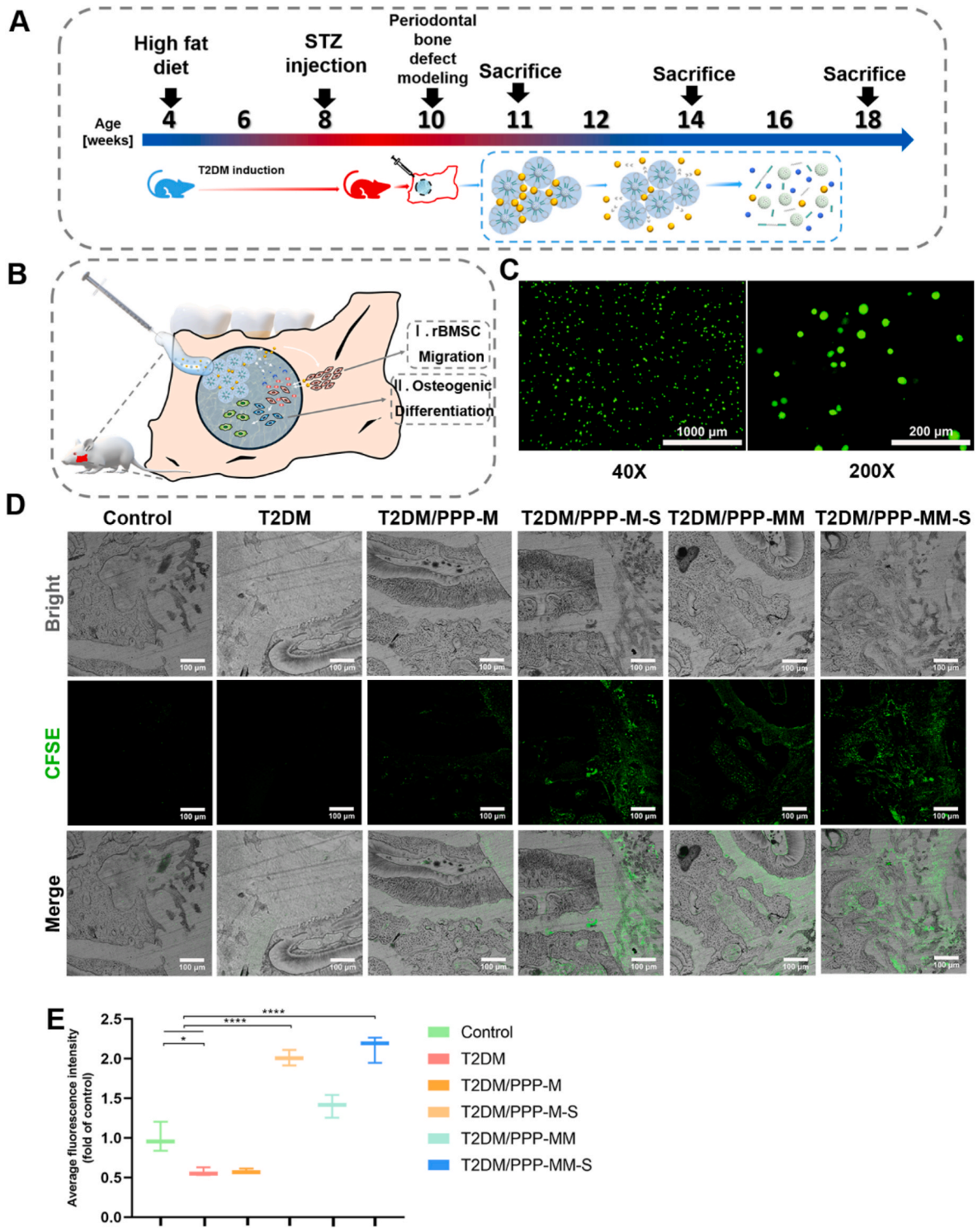

Fig. 6. The drug-delivery system recruited rBMSCs to the periodontal defect in T2DM rats. A) Schematic diagram illustrating the time frame of the *in vivo* study. B) Schematic diagram illustrating the operation process and the expected bone healing cascade with the PPP-MM-S hydrogel. C) Fluorescence microscope images of CFSE-labeled rBMSCs (green) in suspension. D) Confocal fluorescence images of hard tissue sections of periodontal bone defects in healthy (control) and T2DM (type 2 diabetes mellitus) rats to observe the recruited CFSE-labeled rBMSCs (green fluorescence) and E) quantitative analysis of fluorescence intensity. Error bar represents the mean ± SD (n = 3); *, $p < 0.05$; ****, $p < 0.0001$.

foundation for further bone regeneration [38,56].

3.9. Periodontal bone regeneration in vivo

Since the results above demonstrated that the PPP-MM-S drug-delivery system exhibited impressive osteoinductivity in an HG environment *in vitro*, we next applied it to a periodontal defect model in T2DM rats to investigate its bone regenerative capacity *in vivo*.

Fig. 7A shows the 3D reconstructed images of typical samples; new bone in the defect area is marked in yellow. The T2DM control group displayed the least new bone formation, while the normal control group displayed slight new bone formation by self-repair 4 and 8 weeks after

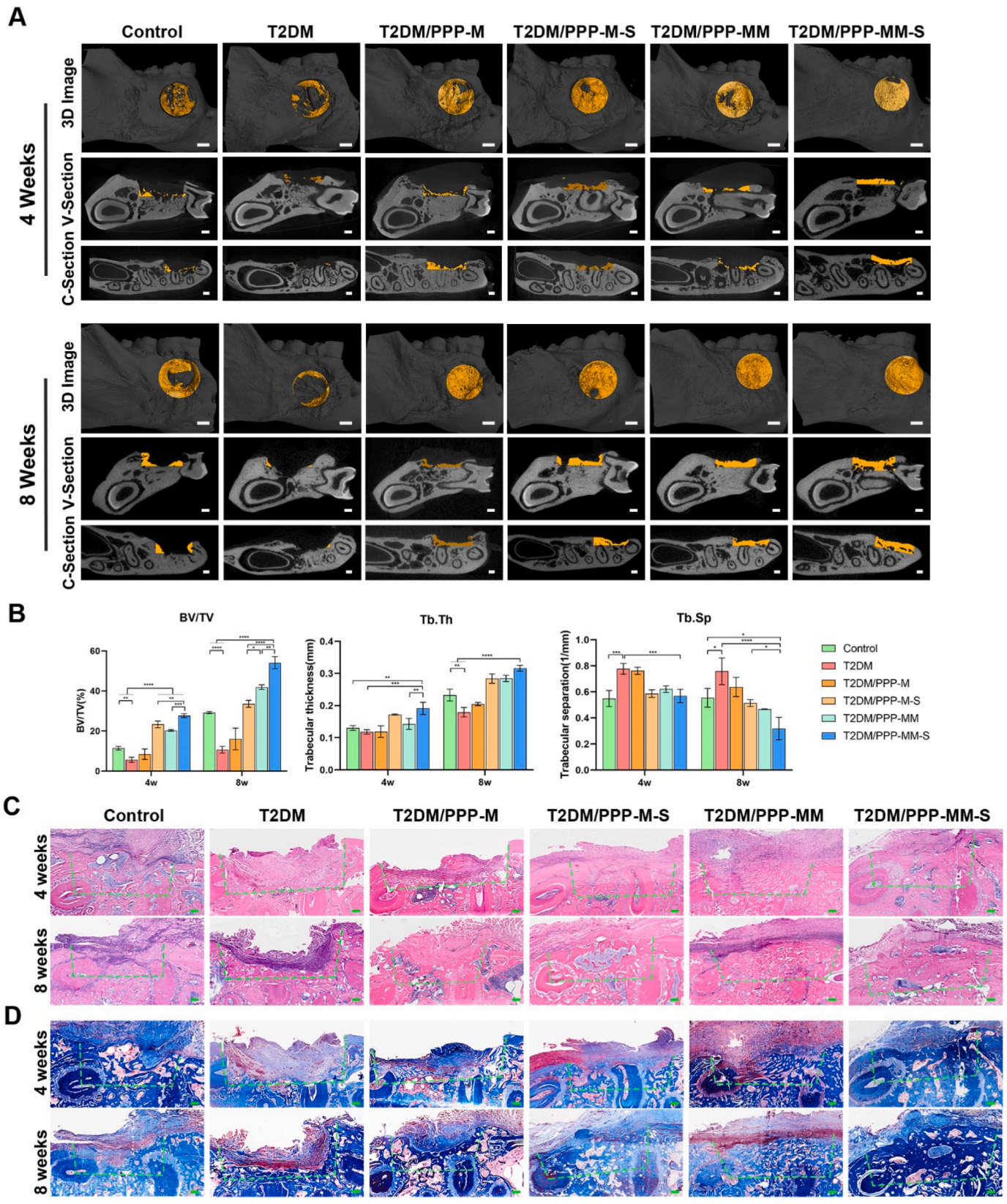

Fig. 7. The drug-delivery system promoted periodontal regeneration in T2DM rats. A) 3D reconstructed, vertical and cross-section images of micro-CT scanning of rat periodontal bone defects implanted with different hydrogels. The new bone in the defect area is marked in yellow. Scale bar: 1 mm. B) Quantitative analysis of bone microarchitectural parameters determined by micro-CT. C). H&E staining images of periodontal bone tissue sections. The defect area is marked with a green dotted line. Scale bar: 300 μm. D). Masson-trichrome staining images of periodontal bone tissue sections. The defect area is marked with a green dotted line. Scale bar: 300 μm. Error bar represents the mean ± SD (n = 3); *, $p < 0.05$; **, $p < 0.01$, ***, $p < 0.001$, ****, $p < 0.0001$.

the operation. Although the differences were not significant, the PPP-M group exhibited slightly more bone regeneration than the two control groups. The three drug-loading groups showed significantly more new bone formation than the other groups. Among them, the PPP-MM-S group displayed the most bone regeneration. The PPP-M-S group showed more new bone regeneration than the PPP-MM group at the 4th week. However, this superiority was reversed at the 8th week. Similar trends among groups could also be observed from the cross and vertical sections of the samples (Fig. 7A). The results of trabecular bone volume fraction (BV/TV) evaluation (Fig. 7B) were essentially consistent with the results of the 3D reconstructed images. Microarchitectural parameters are important indexes that reflect the quality of new bone [57]. As shown in Figs. 7B, 4 and 8 weeks postoperation, the PPP-MM-S group exhibited higher trabecular thickness (Tb. Th), trabecular number (Tb. N) and lower trabecular spacing (Tb. Sp) than the other groups. The values of these three parameters differed among groups in a manner similar to the difference in BV/TV.

H&E and Masson's trichrome staining provided further complementary details regarding the regenerated tissues. As shown in Fig. 7C and D, in accordance with the micro-CT results, 4 weeks after the operation, little new bone could be seen around the edge of the defect in the normal control group, and the defects in the T2DM control and PPP-M groups were mostly filled with fibrous connective tissues. The PPP-MM-S group showed much more new bone formation than the other groups, with blue-stained collagen fibers growing close to the new bone, indicating active bone regeneration. After 8 weeks, in the normal control group, there was still little new bone that could be observed in the defect area. The defects in the T2DM control and PPP-M groups were mostly filled with fibrous connective tissues, although more blue-stained collagen fibers were observed than those observed at the 4th week. More blue-stained new bone formed in the PPP-MM group than in the PPP-M-S group. Moreover, in the PPP-M-S group, although the defects seemed closed from the surface, large and empty areas remained under the closed surface and were filled with some loose connective tissues, suggesting poor osteogenesis and mineralization. The PPP-MM-S group displayed the best bone regeneration, in which the defects were filled with newly formed woven bone with a well-arranged structure, and the irregular new bone on the uneven surface of the defect intersected with blue-stained collagen fibers, suggesting active and ongoing bone remodeling.

Natural bone healing is a well-orchestrated multistage process. A series of secreted growth factors act in a specific succession in this process, activating and coordinating the stages of natural bone regeneration [38,56,58]. During the early phages, it is critical that the defect area recruits enough MSCs with osteogenic potential, which is followed by a signal that induces cell osteogenesis and promotes bone regeneration [59,60]. However, such a "recruitment-osteogenesis" cascade of natural bone healing is significantly depressed in DM [13,61]. This hydrogel-based system was fabricated biomimetically with differential cargo release, which simulated sequentially activated cell-recruitment and osteogenesis biosignals. Specifically, to meet the high demand of the recruiting signal in the initial stage, the SDF-1 quickly escapes from the hydrogel due to diffusion. Simultaneously, to constantly scavenge overproduced ROS in the DM microenvironment and facilitate cell osteogenesis, metformin was first encapsulated in MSNs and then incorporated into the PPP to achieve sustained release. With such a secondary structure, the release of metformin was successfully prolonged to 4 weeks. To date, many strategies, including bone tissue engineering and drug delivery, have been developed to promote periodontal bone regeneration [58,62,63]. However, few of these studies have paid attention to diabetic periodontal bone regeneration. In DM, ROS overproduction leads to disordered bone homeostasis and compromised bone healing, which makes bone regeneration a larger challenge [5,61]. This study proposed a novel bioinspired strategy to promote periodontal bone regeneration under DM conditions, which aimed to reorchestrate the compromised cell migration and osteogenesis stages of bone healing under DM conditions, in the hope of providing an innovative option for diabetic periodontal bone regeneration. Considering that natural bone healing is a very complicated process consisting of various bio-signals (including MSC recruitment, angiogenesis, osteogenesis and so on), we are going to further optimize our system to satisfy the demands of various bio-signals needed in the natural bone healing process in the future.

4. Conclusion

Impaired migration and osteogenic capacities of MSCs in DM make periodontal bone regeneration a major challenge. Inspired by the natural bone healing cascade, we developed a biomimetic PPP-MM-S hydrogel to address the above problems. The hydrogel performed a relatively quick SDF-1 release to recruit early rBMSCs for osteogenesis at the beginning of therapy, and then slowly released metformin in the long term to further promote bone regeneration. Moreover, the hydrogel was potentially able to adapt itself to fit bone defects with any irregular shapes due to its thermosensitive gelation. *In vitro* and *in vivo* experiments indicated that the rapid SDF-1 release from the hydrogel could effectively facilitate MSC migration to the periodontal defect under high glucose conditions, and the subsequently sustained metformin release markedly scavenges the overproduced ROS, which restores osteogenesis via AMPK/β-catenin pathway reactivation under high glucose conditions, resulting in efficient periodontal bone regeneration under T2DM. This work provides a novel therapeutic strategy of a bioinspired drug-delivery system emulating the natural bone healing cascade for diabetic periodontal bone regeneration, which could be extended to the treatment of other types of tissue injuries.

Ethics approval and consent to participate

The animal experiments in this study were conducted according to experimental animal ethics and welfare guidelines approved by the ethics committee of the College of Stomatology, Chongqing Medical University (permit number: CQHS-REC-2020 (LSNo. 76)).

CRediT authorship contribution statement

He Wang: Methodology, Formal analysis, Software, Investigation, Writing – original draft. **Xiaowei Chang:** Methodology, Software, Investigation. **Qian Ma:** Formal analysis, Visualization. **Boyang Sun:** Formal analysis, Visualization. **Han Li:** Resources, Data curation. **Jinmin Zhou:** Validation, Data curation. **Yiyao Hu:** Visualization. **Xiaoyu Yang:** Visualization. **Jie Li:** Conceptualization, Supervision, Writing – review & editing, Resources. **Xin Chen:** Conceptualization, Writing – review & editing, Resources. **Jinlin Song:** Supervision, Project administration, Funding acquisition.

Declaration of competing interest

The authors declare no conflict of interest.

Acknowledgements

This work was supported by the National Natural Science Foundation of China (Grant No. 31971282 and 82071072) and Chongqing Graduate Tutor Team 2019 (dstd201903).

Appendix A. Supplementary data

Supplementary data to this article can be found online at https://doi.org/10.1016/j.bioactmat.2022.08.029.

References

[1] P.I. Eke, L. Wei, W.S. Borgnakke, et al., Periodontitis prevalence in adults ≥ 65 years of age, in the USA, Periodontology 72 (1) (2000) 76–95, 2016.
[2] G. Hajishengallis, T. Chavakis, Local and systemic mechanisms linking periodontal disease and inflammatory comorbidities, Nat. Rev. Immunol. 21 (7) (2021) 426–440.
[3] E. Lalla, P.N. Papapanou, Diabetes mellitus and periodontitis: a tale of two common interrelated diseases, Nat. Rev. Endocrinol. 7 (12) (2011) 738–748.
[4] Z. Hu, C. Ma, X. Rong, et al., Immunomodulatory ECM-like microspheres for accelerated bone regeneration in diabetes mellitus, ACS Appl. Mater. Interfaces 10 (3) (2018) 2377–2390.
[5] K. Wongdee, N. Krishnamra, N. Charoenphandhu, Derangement of calcium metabolism in diabetes mellitus: negative outcome from the synergy between impaired bone turnover and intestinal calcium absorption, J. Physiol. Sci. : JPS 67 (1) (2017) 71–81.
[6] C. Hamann, S. Kirschner, K.-P. Günther, et al., Bone, sweet bone–osteoporotic fractures in diabetes mellitus, Nat. Rev. Endocrinol. 8 (5) (2012) 297–305.
[7] J. Tan, M. Zhang, Z. Hai, et al., Sustained release of two bioactive factors from supramolecular hydrogel promotes periodontal bone regeneration, ACS Nano 13 (5) (2019) 5616–5622.
[8] P.-C. Chang, A.S. Dovban, L.P. Lim, et al., Dual delivery of PDGF and simvastatin to accelerate periodontal regeneration in vivo, Biomaterials 34 (38) (2013) 9990–9997.
[9] A.C. Roberts, J. Gohil, L. Hudson, et al., Aberrant phenotype in human endothelial cells of diabetic origin: implications for saphenous vein graft failure? J. Diabetes Res. 2015 (2015), 409432.
[10] C. Mercier, T. Brazeau, J. Lamoureux, et al., Diabetes impaired ischemia-induced PDGF (Platelet-Derived growth factor) signaling actions and vessel formation through the activation of scr homology 2-containing phosphatase-1, Arterioscler. Thromb. Vasc. Biol. 41 (9) (2021) 2469–2482.
[11] B. Yu, B. Dong, J. He, et al., Bimodal imaging-visible nanomedicine integrating CXCR4 and VEGFa genes directs synergistic reendothelialization of endothelial progenitor cells, Adv. Sci. 7 (24) (2020), 2001657.
[12] W. Ji, F. Yang, J. Ma, et al., Incorporation of stromal cell-derived factor-1α in PCL/gelatin electrospun membranes for guided bone regeneration, Biomaterials 34 (3) (2013) 735–745.
[13] D. Li, K. Chen, H. Tang, et al., A Logic-Based Diagnostic and Therapeutic Hydrogel with Multistimuli Responsiveness to Orchestrate Diabetic Bone Regeneration. Advanced Materials, Deerfield Beach, Fla), 2021, e2108430.
[14] X. Zhao, Y. Yang, J. Yu, et al., Injectable hydrogels with high drug loading through B-N coordination and ROS-triggered drug release for efficient treatment of chronic periodontitis in diabetic rats, Biomaterials 282 (2022), 121387.
[15] C.-H. Tseng, Metformin use is associated with a lower risk of osteoporosis/vertebral fracture in Taiwanese patients with type 2 diabetes mellitus, Eur. J. Endocrinol. 184 (2) (2021) 299–310.
[16] L. Jiating, J. Buyun, Z. Yinchang, Role of metformin on osteoblast differentiation in type 2 diabetes, BioMed Res. Int. 2019 (2019), 9203934.
[17] D. Pankaj, I. Sahu, I.G. Kurian, et al., Comparative evaluation of subgingivally delivered 1.2% rosuvastatin and 1% metformin gel in treatment of intrabony defects in chronic periodontitis: a randomized controlled clinical trial, J. Periodontol. 89 (11) (2018) 1318–1325.
[18] Y. Kuang, B. Hu, G. Feng, et al., Metformin prevents against oxidative stress-induced senescence in human periodontal ligament cells, Biogerontology 21 (1) (2020) 13–27.
[19] B. Sun, S. Ying, Q. Ma, et al., Metformin Ameliorates HMGB1-Mediated Oxidative Stress through mTOR Pathway in Experimental Periodontitis, Genes & Diseases, 2021.
[20] E.G. Buettmann, J.A. McKenzie, N. Migotsky, et al., VEGFA from early osteoblast lineage cells (Osterix+) is required in mice for fracture healing, J. Bone Miner. Res. : Off. J. Am. Soc. Bone Min. Res. 34 (9) (2019) 1690–1706.
[21] L.Y. Chong, L.-Y. Chien, M.-C. Chung, et al., Controlling the proliferation and differentiation stages to initiate periodontal regeneration, Connect. Tissue Res. 54 (2) (2013) 101–107.
[22] M.K. Nguyen, E. Alsberg, Bioactive factor delivery strategies from engineered polymer hydrogels for therapeutic medicine, Prog. Polym. Sci. 39 (7) (2014) 1236–1265.
[23] N.J. Shah, M.N. Hyder, M.A. Quadir, et al., Adaptive growth factor delivery from a polyelectrolyte coating promotes synergistic bone tissue repair and reconstruction, in: Proceedings of the National Academy of Sciences of the United States of America, vol. 111, 2014, pp. 12847–12852, 35.
[24] S. Eskandari, T. Guerin, I. Toth, et al., Recent advances in self-assembled peptides: implications for targeted drug delivery and vaccine engineering, Adv. Drug Deliv. Rev. 110–111 (2017) 169–187.
[25] S. Chava, S. Chennakesavulu, B.M. Gayatri, et al., A novel phosphorylation by AMP-activated kinase regulates RUNX2 from ubiquitination in osteogenesis over adipogenesis, Cell Death Dis. 9 (7) (2018) 754.
[26] L. Yu, H. Liang, X. Dong, et al., Reduced silent information regulator 1 signaling exacerbates myocardial ischemia-reperfusion injury in type 2 diabetic rats and the protective effect of melatonin, J. Pineal Res. 59 (3) (2015) 376–390.
[27] M. Kleinert, C. Clemmensen, S.M. Hofmann, et al., Animal models of obesity and diabetes mellitus, Nat. Rev. Endocrinol. 14 (3) (2018) 140–162.
[28] M. Padial-Molina, J.C. Rodriguez, S.L. Volk, et al., Standardized in vivo model for studying novel regenerative approaches for multitissue bone-ligament interfaces, Nat. Protoc. 10 (7) (2015) 1038–1049.
[29] K. Shi, Y.-L. Wang, Y. Qu, et al., Synthesis, characterization, and application of reversible PDLLA-PEG-PDLLA copolymer thermogels in vitro and in vivo, Sci. Rep. 6 (2016), 19077.
[30] B.-B. Seo, J.-T. Koh, S.-C. Song, Tuning Physical Properties and BMP-2 Release Rates of Injectable Hydrogel Systems for an Optimal Bone Regeneration Effect, Biomaterials, 2017, p. 122.
[31] S. Fakhruddin, W. Alanazi, K.E. Jackson, Diabetes-induced reactive oxygen species: mechanism of their generation and role in renal injury, J. Diabetes Res. 2017 (2017), 8379327.
[32] D. Haspula, A.K. Vallejos, T.M. Moore, et al., Influence of a hyperglycemic microenvironment on a diabetic versus healthy rat vascular endothelium reveals distinguishable mechanistic and phenotypic responses, Front. Physiol. 10 (2019) 558.
[33] R.A. DeFronzo, E. Ferrannini, L. Groop, et al., Type 2 diabetes mellitus, Nat. Rev. Dis. Prim. 1 (2015), 15019.
[34] Y.-F. Feng, L. Wang, Y. Zhang, et al., Effect of reactive oxygen species overproduction on osteogenesis of porous titanium implant in the present of diabetes mellitus, Biomaterials 34 (9) (2013) 2234–2243.
[35] Q. He, S. Yuan, H. Tang, et al., Safeguarding osteointegration in diabetic patients: a potent "chain armor" coating for scavenging ROS and macrophage reprogramming in a microenvironment-responsive manner, Adv. Funct. Mater. 31 (31) (2021), 2101611.
[36] R. Zhou, Y. Ma, S. Qiu, et al., Metformin promotes cell proliferation and osteogenesis under high glucose condition by regulating the ROS-AKT-mTOR axis, Mol. Med. Rep. 22 (4) (2020) 3387–3395.
[37] J. Chen, Y. Zhang, P. Pan, et al., In situ strategy for bone repair by facilitated endogenous tissue engineering, Colloids Surf. B Biointerfaces 135 (2015) 581–587.
[38] M.M. Martino, P.S. Briquez, K. Maruyama, et al., Extracellular matrix-inspired growth factor delivery systems for bone regeneration, Adv. Drug Deliv. Rev. 94 (2015) 41–52.
[39] T. Ding, J. Li, X. Zhang, et al., Super-assembled core/shell fibrous frameworks with dual growth factors for in situ cementum-ligament-bone complex regeneration, Biomater. Sci. 8 (9) (2020) 2459–2471.
[40] Y.-W. Won, A.N. Patel, D.A. Bull, Cell surface engineering to enhance mesenchymal stem cell migration toward an SDF-1 gradient, Biomaterials 35 (21) (2014) 5627–5635.
[41] Y. Yang, Y. Zhou, Y. Wang, et al., Exendin-4 reverses high glucose-induced endothelial progenitor cell dysfunction via SDF-1β/CXCR7-AMPK/p38-MAPK/IL-6 axis, Acta Diabetol. 57 (11) (2020) 1315–1326.
[42] Y. Weng, J. Lou, X. Liu, et al., Effects of high glucose on proliferation and function of circulating fibrocytes: involvement of CXCR4/SDF-1 axis, Int. J. Mol. Med. 44 (3) (2019) 927–938.
[43] A.J. Whittam, Z.N. Maan, D. Duscher, et al., Small molecule inhibition of dipeptidyl peptidase-4 enhances bone marrow progenitor cell function and angiogenesis in diabetic wounds, Transl. Res. : J. Lab. Clin. Med. 205 (2019) 51–63.
[44] Y. Sun, Y. Zhu, X. Liu, et al., Morroniside attenuates high glucose-induced BMSC dysfunction by regulating the Glo1/AGE/RAGE axis, Cell Prolif 53 (8) (2020), e12866.
[45] M. Shah, B. Kola, A. Bataveljic, et al., AMP-activated protein kinase (AMPK) activation regulates in vitro bone formation and bone mass, Bone 47 (2) (2010) 309–319.
[46] T. Jiang, C. Xia, X. Chen, et al., Melatonin promotes the BMP9-induced osteogenic differentiation of mesenchymal stem cells by activating the AMPK/β-catenin signalling pathway, Stem Cell Res. Ther. 10 (1) (2019) 408.
[47] C.N. Bennett, K.A. Longo, W.S. Wright, et al., Regulation of osteoblastogenesis and bone mass by Wnt10b, in: Proceedings of the National Academy of Sciences of the United States of America, vol. 102, 2005, pp. 3324–3329, 9.
[48] T. Gaur, C.J. Lengner, H. Hovhannisyan, et al., Canonical WNT signaling promotes osteogenesis by directly stimulating Runx2 gene expression, J. Biol. Chem. 280 (39) (2005) 33132–33140.
[49] R. Baron, M. Kneissel, WNT signaling in bone homeostasis and disease: from human mutations to treatments, Nat. Med. 19 (2) (2013) 179–192.
[50] L. Qu, N. Dubey, J.S. Ribeiro, et al., Metformin-loaded nanospheres-laden photocrosslinkable gelatin hydrogel for bone tissue engineering, J. Mech. Behav. Biomed. Mater. 116 (2021), 104293.
[51] J.W. Brown, C.J. Cho, Mills J.C. Paligenosis, Cellular remodeling during tissue repair, Annu. Rev. Physiol. 84 (2022) 461–483.
[52] T. Komori, H. Yagi, S. Nomura, et al., Targeted disruption of Cbfa1 results in a complete lack of bone formation owing to maturational arrest of osteoblasts, Cell 89 (5) (1997) 755–764.
[53] K. Nakashima, X. Zhou, G. Kunkel, et al., The novel zinc finger-containing transcription factor osterix is required for osteoblast differentiation and bone formation, Cell 108 (1) (2002) 17–29.
[54] D.M. Reffitt, N. Ogston, R. Jugdaohsingh, et al., Orthosilicic acid stimulates collagen type 1 synthesis and osteoblastic differentiation in human osteoblast-like cells in vitro, Bone 32 (2) (2003) 127–135.
[55] L.N. Luong, J. Ramaswamy, D.H. Kohn, Effects of osteogenic growth factors on bone marrow stromal cell differentiation in a mineral-based delivery system, Biomaterials 33 (1) (2012) 283–294.
[56] M. Mehta, K. Schmidt-Bleek, G.N. Duda, et al., Biomaterial delivery of morphogens to mimic the natural healing cascade in bone, Adv. Drug Deliv. Rev. 64 (12) (2012) 1257–1276.
[57] N. Kimelman-Bleich, G. Pelled, D. Sheyn, et al., The use of a synthetic oxygen carrier-enriched hydrogel to enhance mesenchymal stem cell-based bone formation in vivo, Biomaterials 30 (27) (2009) 4639–4648.

[58] S. Herberg, A.M. McDermott, P.N. Dang, et al., Combinatorial morphogenetic and mechanical cues to mimic bone development for defect repair, Sci. Adv. 5 (8) (2019), eaax2476.
[59] R.C.H. Gresham, C.S. Bahney, J.K. Leach, Growth factor delivery using extracellular matrix-mimicking substrates for musculoskeletal tissue engineering and repair, Bioact. Mater. 6 (7) (2021) 1945–1956.
[60] V.P. Shastri, In vivo engineering of tissues: biological considerations, challenges, strategies, and future directions, Adv. Mater. 21 (32–33) (2009) 3246–3254.
[61] X. Sun, Z. Ma, X. Zhao, et al., Three-dimensional bioprinting of multicell-laden scaffolds containing bone morphogenic protein-4 for promoting M2 macrophage polarization and accelerating bone defect repair in diabetes mellitus, Bioact. Mater. 6 (3) (2021) 757–769.
[62] Z.-K. Cui, S. Kim, J.J. Baljon, et al., Design and characterization of a therapeutic non-phospholipid liposomal nanocarrier with osteoinductive characteristics to promote bone formation, ACS Nano 11 (8) (2017) 8055–8063.
[63] D. Khare, B. Basu, A.K. Dubey, Electrical stimulation and piezoelectric biomaterials for bone tissue engineering applications, Biomaterials 258 (2020), 120280.